Effect of isolated fractures on accelerated flow in unsaturated porous rock

Grace W. Su[1] and John R. Nimmo
U.S. Geological Survey, Menlo Park, California, USA

Maria I. Dragila
Department of Crop and Soil Science, Oregon State University, Corvallis, Oregon, USA

Received 27 August 2002; revised 25 August 2003; accepted 17 September 2003; published 2 December 2003.

[1] Fractures that begin and end in the unsaturated zone, or isolated fractures, have been ignored in previous studies because they were generally assumed to behave as capillary barriers and remain nonconductive. We conducted a series of experiments using Berea sandstone samples to examine the physical mechanisms controlling flow in a rock containing a single isolated fracture. The input fluxes and fracture orientation were varied in these experiments. Visualization experiments using dyed water in a thin vertical slab of rock were conducted to identify flow mechanisms occurring due to the presence of the isolated fracture. Two mechanisms occurred: (1) localized flow through the rock matrix in the vicinity of the isolated fracture and (2) pooling of water at the bottom of the fracture, indicating the occurrence of film flow along the isolated fracture wall. These mechanisms were observed at fracture angles of 20 and 60 degrees from the horizontal, but not at 90 degrees. Pooling along the bottom of the fracture was observed over a wider range of input fluxes for low-angled isolated fractures compared to high-angled ones. Measurements of matrix water pressures in the samples with the 20 and 60 degree fractures also demonstrated that preferential flow occurred through the matrix in the fracture vicinity, where higher pressures occurred in the regions where faster flow was observed in the visualization experiments. The pooling length at the terminus of a 20 degree isolated fracture was measured as a function of input flux. Calculations of the film flow rate along the fracture were made using these measurements and indicated that up to 22% of the flow occurred as film flow. These experiments, apparently the first to consider isolated fractures, demonstrate that such features can accelerate flow through the unsaturated zone and should be considered when developing conceptual models. *INDEX TERMS:* 1829 Hydrology: Groundwater hydrology; 1832 Hydrology: Groundwater transport; 1875 Hydrology: Unsaturated zone; *KEYWORDS:* unsaturated flow, fractured rock, preferential flow

Citation: Su, G. W., J. R. Nimmo, and M. I. Dragila, Effect of isolated fractures on accelerated flow in unsaturated porous rock, *Water Resour. Res.*, *39*(12), 1326, doi:10.1029/2002WR001691, 2003.

1. Introduction

[2] Understanding flow processes in the unsaturated zone is critical since the introduction of contaminants often occurs in this region. Fractures and macropores are common in the unsaturated zone and have a significant effect on contaminant transport. Field studies have demonstrated that flow can occur preferentially through fractures in the unsaturated zone, resulting in transport times much faster than predicted by conventional models based on Richards' equation [e.g., *Nativ et al.*, 1995; *Dahan et al.*, 1999; *Faybishenko et al.*, 2000]. Our understanding of mechanisms controlling flow through fractured media is limited, however. Flow processes that may occur in fractures include saturated plug flow [*Nitao and Buscheck*, 1991], fingering [*Nicholl et al.*, 1994], film flow [*Tokunaga and Wan*, 1997], and intermittent flow [*Glass and Nicholl*, 1996; *Su et al.*, 1999]. Another possible mechanism is preferential flow along a fracture coating with a higher permeability than the bulk matrix [*Tokunaga and Wan*, 2001].

[3] Research efforts to bridge the gap between conventional model predictions and field observations have largely focused on fractures that are open to the land surface [e.g., *Nitao and Buscheck*, 1991; *Tidwell et al.*, 1995; *Soll and Birdsell*, 1998] where precipitation can infiltrate and be readily transported through the unsaturated zone. In deep unsaturated zones, fracture networks that are open to the land surface are likely to dead-end or become filled before reaching the groundwater table. Isolated fractures, or fractures that begin and end in the unsaturated zone (Figure 1), may be common in these regions and may play an important role in transport. These features have generally been ignored in unsaturated zone flow since they are assumed to act as

[1]Now at Lawrence Berkeley National Laboratory, Berkeley, California, USA.

0043-1397/03/2002WR001691$09.00

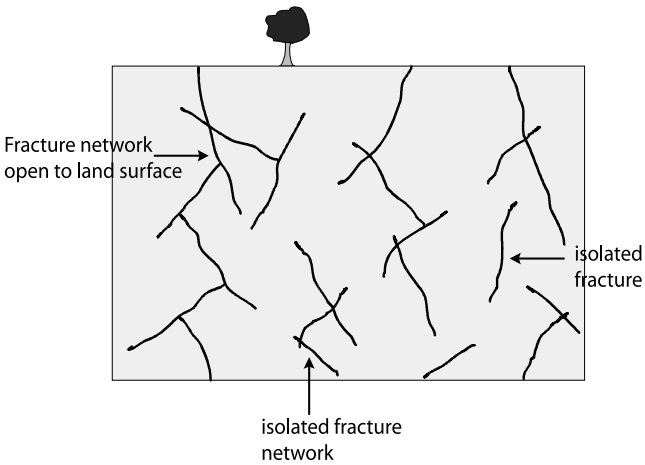

Figure 1. Schematic of subsurface containing isolated fractures and fractures open to the land surface.

barriers to flow [*Wang and Narasimhan*, 1985], provided that the apertures are large relative to pores in the surrounding matrix. Wide-aperture fractures, defined here as fractures with apertures greater than 1 mm, are generally assumed to be nonconductive since water does not span the aperture. Isolated fractures could be key structures in the development of accelerated paths in fractured unsaturated zones. *Dragila* [1999] developed a field-scale model that consisted of flow occurring through the rock matrix and a series of isolated fractures. Flow through the fractures was conceptualized to occur along films in this model. This model successfully reproduced the travel times of the bomb pulse chlorine-36 measured at Yucca Mountain [*Fabryka-Martin et al.*, 1996].

[4] Possible mechanisms generating fast flow near isolated fractures are illustrated in Figure 2. Flow through the rock matrix may become funneled due to the presence of an isolated fracture, forming local regions of higher saturation above and around the fracture. A similar concept is examined in numerical simulations conducted by *Birkholzer et al.* [1999], where a region of higher water saturation forms in the rock matrix above and to the sides of a tunnel idealized as a circular opening. They called this phenomenon the shadow effect because a stagnation point develops below the tunnel where the saturation in the matrix is lower than the saturation surrounding the tunnel. The shadow diminishes, however, if seepage enters the tunnel. The seepage criterion into openings of different shapes, including a circular one, was derived by *Philip* [1989]. Another possible fast flow mechanism is thick film flow along the fracture wall, where a film is defined as having one contact and one free surface. A thick film has a thickness greater than 1 μm [*Tokunaga and Wan*, 1997, 2001]. If the film is more conductive than the rock matrix, pooling of water at the terminus of the fracture may also occur. Film flow has been demonstrated to occur along the fracture surface when water pressures in the rock matrix are close to zero [*Tokunaga and Wan*, 1997]. The possibility of film flow occurring along isolated fractures has not been examined, however. When fractures are isolated, the formation of a saturated region (and pressures near zero) in the matrix above the fracture may generate a free-surface film on the fracture wall, provided that the fracture is relatively wide.

[5] The objective of this study is to determine the effect that wide-aperture isolated fractures have on the development of accelerated flow paths through the unsaturated zone. Wide-aperture fractures are examined because they have been ignored in previous studies and are likely to generate physical mechanisms for rapid transport not previously investigated. Flow visualization experiments are conducted on a porous rock containing a single isolated fracture to obtain qualitative information on the flow movement. Rock matrix pressure measurements are made and compared to the results of the visual observations. Calculations of film flow along an isolated fracture are presented and used to characterize experimental results.

2. Experimental Approach

[6] Experiments were conducted at room temperature (~20°C) on rectangular slabs of Berea sandstone (Cleveland quarries; Cleveland, Ohio) with dimensions 10 × 15 × 0.6 cm and a nominal permeability of 10^{-13} m^2 as measured by the supplier. Berea sandstone was used because we are interested in investigating the effect of isolated fractures in a permeable rock with a homogenous matrix. Although thin laminations were present in the Berea sandstone samples, the wetting front was uniform as water imbibed into the dry sample, and the rock was assumed to be nearly homogeneous. A drop of water placed on the dry rock immediately imbibed into it, indicating that the rock was strongly wetting. A slit was cut through the center of each sample using a Dremel diamond wheel to create an isolated fracture 1–2 mm wide, about 6 cm long, and oriented at an angle in the range of 20 to 90 degrees from the horizontal. A range of angles was used to investigate the influence of fracture inclination on flow. An aperture width greater than 1 mm was chosen to be large enough to prevent flow across the fracture.

[7] The initially air-filled pores in the rock sample were saturated with deaired distilled water before delivering water to it at a constant flux by means of a syringe pump. A flux less than the saturated hydraulic conductivity of the sample (10^{-4} cm/s) was applied to establish unsaturated conditions. After conditions in the sample were steady

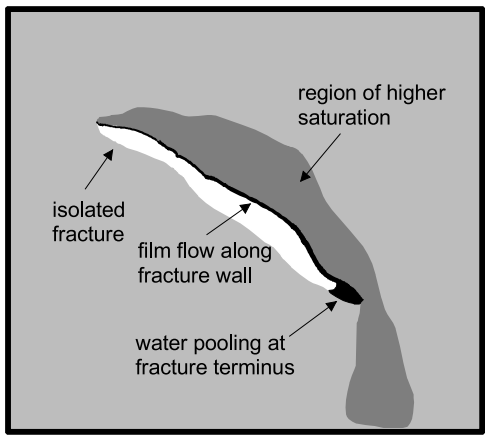

Figure 2. Possible flow processes occurring in a rock containing an isolated fracture.

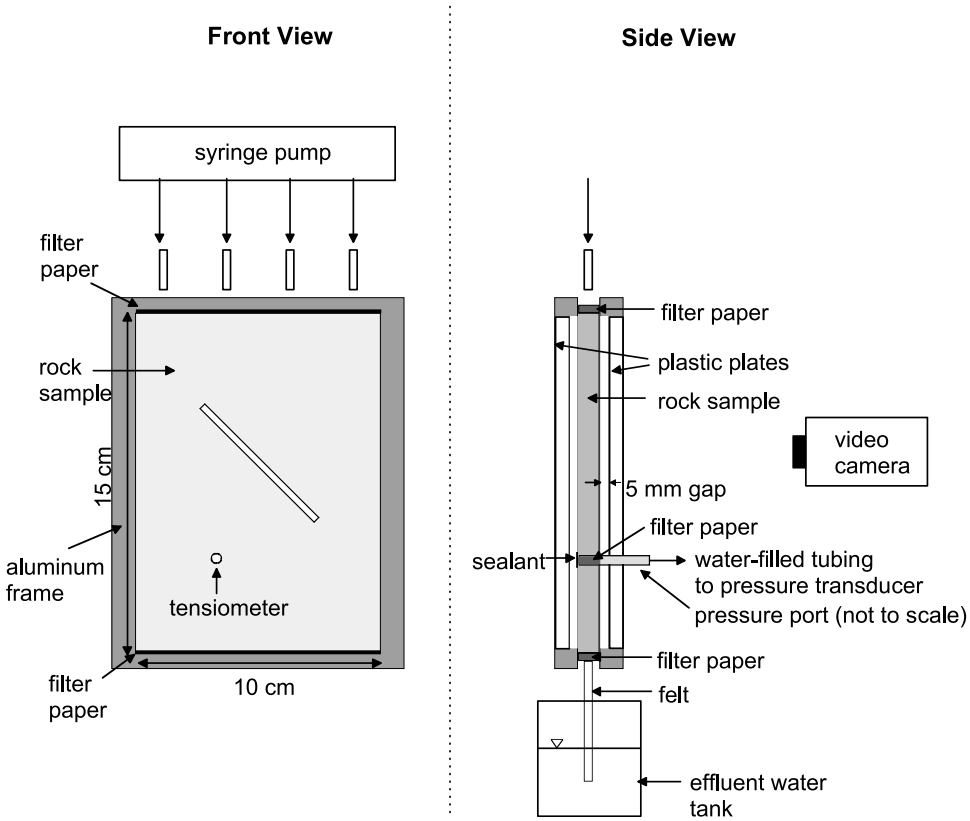

Figure 3. Schematic of experimental apparatus.

(approximately 24–48 hours), water containing a fluorescein dye at a concentration of 0.5 g/L was introduced to the sample. Fluorescein dye was selected for its low retardation factor. Ultraviolet light was used to help visualize the liquid movement through the sample. A digital video camera recorded observations of the liquid movement. To permit visualization of the dye, the outside faces of the sample were not sealed. Implications of using an unsealed sample are discussed in the results section. A schematic of the apparatus used to conduct these experiments is shown in Figure 3. A thin strip of filter paper at the sample inlet distributed water across the sample width. At the outlet, a strip of filter paper and a piece of felt drained water out of the sample. The sample was placed in an aluminum frame, bolted on the sides, and mounted vertically for the experiments. Plastic plates placed over the front and back faces of the sample minimized evaporation. Clearance of about 0.5 cm between the plastic plate and the rock sample prevented flow between the plate and the sample. No confining pressure was used on the sample. After completing the visualization experiment, the sample was removed from the aluminum frame and immersed in clean distilled water to remove the dye. The sample was then air dried and prepared in the same manner as just described when the experiment was repeated.

[8] Matrix pressure measurements were made in samples containing a fracture oriented at 20, 60, and 90 degrees. Holes with a diameter of approximately 3 mm were drilled through each sample at seven points. The locations of the seven pressure ports in the two samples are shown in a subsequent figure (Figure 8). The holes were filled with saturated filter paper with a nominal pore size of 0.7 μm and then the backsides of the holes were sealed. The filter paper was connected to a pressure transducer by water-filled tubing, creating a tensiometer. Pressures were measured initially for a flux of 9.2×10^{-5} cm/s and then for fluxes of 5.6×10^{-5} cm/s and 3.7×10^{-5} cm/s in samples with the 20 and 60 degree fracture. Fluxes of 9.2×10^{-5}, 7.6×10^{-5}, and 5.6×10^{-5} cm/s were used in the sample with the 90 degree fracture. The system equilibrated to each flux for 24–48 hours before pressure measurements were made.

3. Results

3.1. Flow Visualization Experiments

[9] Figure 4 contains images of the dyed water moving with an input flux of 7.1×10^{-5} cm/s through a slab of Berea sandstone with a fracture oriented 60 degrees from the horizontal. The time indicates minutes after dyed water was introduced into the sample. The results demonstrate that flow becomes localized through the rock matrix because of the presence of the isolated fracture, occurring preferentially along the top of the fracture and to the right side of the sample. Results from a higher input flux of 9.2×10^{-5} cm/s are shown in Figure 5, where pooling of water at the terminus of the fracture is observed in addition to preferential flow in the matrix. The two fluxes bracketed the transition between flow with and without pooling. Pooling indicates the development of a free-surface film along the isolated fracture and occurs when the film is more conductive than the local rock matrix. Although water did not accumulate at the end of the fracture for an input flux of 7.1×10^{-5} cm/s, a film less

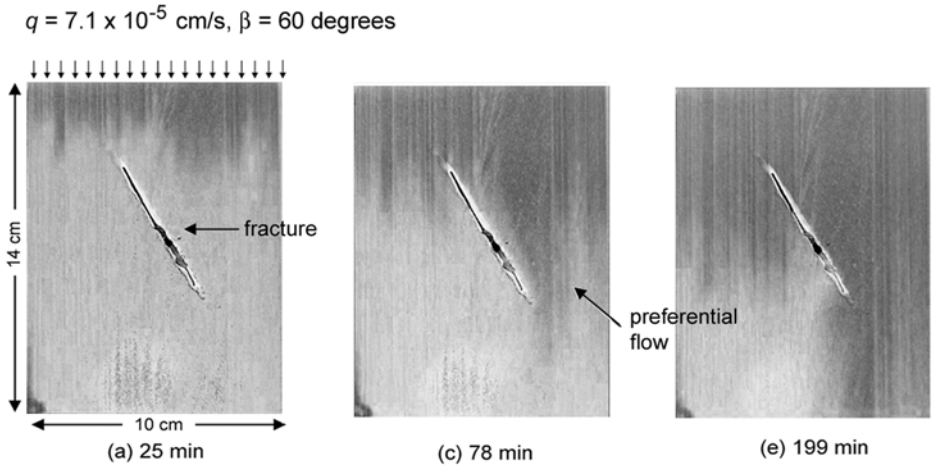

Figure 4. Water movement (green) through a slab of Berea sandstone containing a 60 degree isolated fracture. Time indicates minutes after dyed water was introduced into the sample. The q is the imposed flux density and β is the fracture angle from the horizontal. See color version of this figure at back of this issue.

conductive than the local matrix may have still been present but been too thin to be observed.

[10] Preferential flow through the rock matrix also occurred in a sample with an isolated fracture at 20 degrees. Flow was diverted around the isolated fracture, resulting in preferential flow both to the left and right of the fracture (Figure 6). In a sample with a fracture at 90 degrees, flow was nearly uniform down the sample (Figure 7), indicating that flow localization in the rock matrix only occurs in samples with an inclined fracture. At a flux of 9.2×10^{-5} cm/s, pooling of water at the terminus of the fracture was observed in the 20 and 60 degree isolated fractures, but not in the 90 degree fracture. If film flow was occurring along the walls of the 90 degree fracture, the film must have been less conductive than the matrix. In addition, the observed pool length in the sample with the 20 degree fracture was longer than the pool length in the 60 degree fracture at a flux of 9.2×10^{-5} cm/s, indicating that the film flux was larger along the 20 degree fracture.

[11] In experiments repeated on the same three rock samples, preferential flow was again observed in the samples with the 20 and 60 degree fractures, but not in the sample with the 90 degree fracture. Although the locations of the flow paths in the repeat experiments were similar to the results presented in Figures 4–7, the rates of dye advancement differed by up to a factor of 1.5. Flow is sensitive to even slight changes in the initial and boundary conditions, and it is difficult to keep these conditions identical in different experiments. Since the rock was not deaired prior to saturating it with water, the amount of entrapped air may have changed when the same sample was used in a repeat experiment. The rate that water flows through the rock sample is reduced in regions with more entrapped air. Slight differences in the rate that water was delivered to the sample by the syringe pump may have also contributed to the different rates of dye advancement.

[12] In the experiments, the external, vertical faces of the rock sample were not sealed, so water could potentially flow through the rock matrix as well as along films on the faces. Along some portions of the rock face, the rate at which the dye advanced in Figures 4–7 was larger than the calculated saturated pore velocity for this sandstone ($\sim 5 \times 10^{-4}$ cm/s, using a porosity of 0.20), indicating the advancement of dye along external films rather than the matrix.

[13] The volumetric flux of water moving down the outside faces of the slab can be calculated by

$$Q = 2(\delta D u) \tag{1}$$

where δ is the film thickness, D is the horizontal dimension of the sample, and u is the film velocity. The factor of 2 in the equation above takes into account film flow along the front and back faces. Although the film thickness and velocity are variable on the rock faces, we will calculate the maximum volumetric flux of water moving down the faces

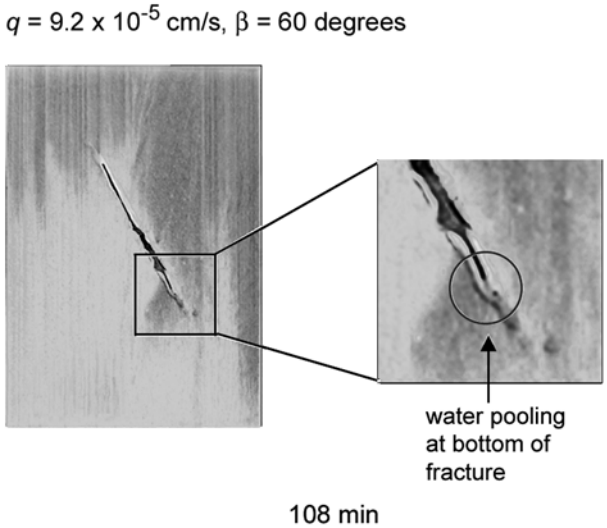

Figure 5. Water pooling at the terminus of the fracture, indication of development of free-surface film flow along the fracture walls. See color version of this figure at back of this issue.

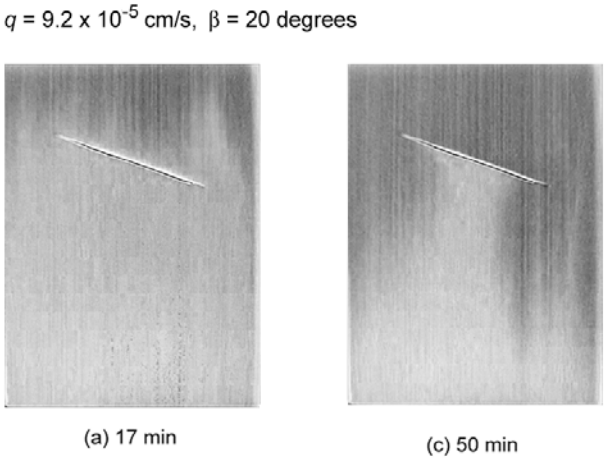

Figure 6. Flow occurs preferentially along the left and right sides of a sample containing a 20 degree isolated fracture. See color version of this figure at back of this issue.

by using the largest film velocity, obtained by measuring the largest distance traveled by the dye front in the least amount of time between two subsequent images (Figures 4–7). The film thickness corresponding to this velocity can be calculated using the equation derived for a falling film on a smooth surface [*Bird et al.*, 1960]:

$$\delta = \left(u \left(\frac{3\mu}{\rho g \sin\beta} \right) \right)^{1/2} \tag{2}$$

where μ is the viscosity of water, ρ is the density of water, g is the gravitational acceleration, and β is the fracture inclination angle. The maximum film velocity measured in the visualization experiments was approximately 3.5×10^{-3} cm/s, corresponding to a film thickness of 3.3 microns. Using equation (1) and the calculated film thickness, the maximum flow rate along the films on the walls is 2.3×10^{-5} cm^3/s. This is about 4% of the total input flux of 5.5×10^{-4} cm^3/s (9.2×10^{-5} cm/s $\times$ 10 cm $\times$ 0.6 cm), indicating that the amount of flow occurring as films on the vertical faces is relatively small.

3.2. Localized Flow Through Rock Matrix: Pressure Measurements

[14] Water pressure measurements were made to further characterize preferential flow caused by an isolated fracture. The location of the seven pressure ports in the three Berea sandstone samples and the corresponding plots of the pressure as a function of flux for each of the samples are presented in Figures 8a–8c. One set of pressure measurements for each rock sample is presented in Figure 8, illustrating the typical pressure trend observed due to the presence of the isolated fracture. The pressures in the seven ports measured in the sample with a 20 degree fracture are shown in Figure 8a. As expected, the water pressures generally decrease with decreasing flux. At 9.2×10^{-5} cm/s, the pressures in all seven ports are nearly the same, but at 5.6×10^{-5} cm/s the pressure differences in the seven ports become more significant. The pressures above the isolated fracture in ports 1, 2, and 4 do not decrease as much with decreasing flux as the pressures in the ports below. The pressures in ports 1 and 2 are also nearly identical to each other at the different input fluxes, which indicates that flow occurs uniformly through the top of the sample before reaching the isolated fracture. The pressures in port 4, immediately above the fracture, remain nearly constant at approximately -0.3 cm. This pressure is higher than the pressures in the other ports as the flux decreases. The pressures in port 3 and in ports 5–7 decrease with decreasing flux, with a larger drop in pressure as the flux decreases from 5.6×10^{-5} to 3.7×10^{-5} cm/s. The pressures in ports 5 and 7 are slightly higher than port 6, consistent with the visualization experiments where flow occurred preferentially on the left and right sides immediately below the fracture.

[15] Figure 8b contains plots of the pressure as a function of flux for the sample with a fracture at 60 degrees. The pressures in ports 1 and 2 are nearly the same at the different input fluxes, which again indicates that flow is uniform before reaching the isolated fracture. The effect of the isolated fracture on matrix pressures is evident when comparing the pressures in ports 3–5. The pressure in port 3 is consistently less than ports 4 and 5 at all fluxes. At the bottom of the sample, the pressure in port 6 is also less than port 7 as a function of flux. If the sample is unsaturated, these results indicate that the saturation is higher on the right side of the sample, corresponding to the faster flow path observed in the visualization experiments. These results are also consistent with expectations based on conservation of mass, where a region of higher flow on the right requires there to be a region of lower flow on the left.

[16] The pressures measured in the sample with a fracture at 90 degrees are presented in Figure 8c. The pressures in the seven ports remain nearly constant as the flux decreases from 9.2×10^{-5} to 7.7×10^{-5} cm/s, but then they decrease at a flux of 5.6×10^{-5} cm/s. The ports aligned along the same y-coordinate have nearly the same pressures,

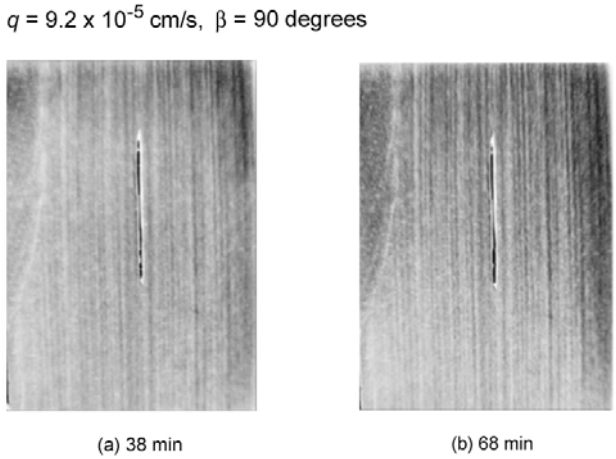

Figure 7. Flow occurs nearly uniformly along a sample containing a 90 degree isolated fracture. See color version of this figure at back of this issue.

indicating that the flow is nearly uniform across the sample, which is consistent with the visualization experiments. The decrease in the pressures with depth is due to the pressure difference between the top and bottom of the sample.

[17] Even though the input fluxes used in these experiments were less than the saturated hydraulic conductivity of the sandstone, the matrix may be saturated at the higher fluxes. We will assume that the differences in matrix pressures relative to the isolated fracture will remain qualitatively the same if the matrix is unsaturated. In the samples with the 20 and 60 degree fractures, higher matrix pressures were measured in the region above the fracture compared to below it at nearly all the fluxes, indicating that in an unsaturated matrix, a region of higher saturation will generally be found above an inclined isolated fracture. The main difference in these samples occurred at a flux of 3.7×10^{-5} cm/s where the pressures measured above the fracture at 20 degrees were higher than those with the fracture at 60 degrees. This difference suggests that the matrix above the fracture would remain wetter over a larger range of fluxes for low-angled fractures compared to higher-angled ones.

3.3. Quantification of Film Flow in Isolated Fractures

[18] The previous section examined the impact of an isolated fracture on preferential flow. An additional observation in the visualization experiments was pooling of water at the bottom of the fracture, indicating film flow occurring along the fracture. Quantification of film flow gives insight into the conditions giving rise to it.

3.3.1. Theoretical Formulation

[19] *Tokunaga and Wan* [1997] presented a theory for film flow along the surfaces of large-aperture fractures and demonstrated in laboratory experiments that this can occur when the matrix pressures are close to zero. *Or and Tuller* [2000] derived a theoretical expression for the hydraulic conductivity of films on a rough fracture surface and found that their calculations agreed well with the results of *Tokunaga and Wan* [1997]. These studies, however, did not discuss the possibility of film flow occurring along isolated fractures.

[20] Flow lines in a rock containing an isolated fracture are drawn schematically in Figure 9. Water will flow primarily vertically through the matrix, except near the fracture-matrix interface, where some flow will be diverted laterally due to the presence of the fracture. A film along the fracture surface may also be generated when water exits the matrix along the interface. The source flow rate for the film as a function of distance along the fracture, x', is calculated by

$$Q(x')_{\text{source}} = \int_0^{x'} q_v W dx' \tag{3}$$

where q_v is the seepage flux density exiting the matrix at the interface and W is the thickness of the sample. Since the source feeds into the film over the length of the fracture, the thickness and velocity of the film will increase with distance.

[21] In our experiments, pooling of water at the terminus of the fracture was used as an indication of film flow and occurred for some input fluxes and fracture inclinations. Assuming that q_v is uniform over the length of the fracture and that water feeds into the film beginning at the top of the fracture ($x' = 0$) to the start of the pool ($x' = L - L_{\text{pool}}$), the volumetric flux of the film entering this pool ($Q_{\text{film,in}}$) can be calculated using the following equation:

$$Q_{\text{film,in}} = q_v W (L - L_{\text{pool}}) \tag{4}$$

where L is the entire fracture length and L_{pool} is the pool length (see Figure 9). The pool length was observed to remain constant over time when the flow through the sample had reached steady state, indicating that the flux entering the pool is equal to the flux out of the pool. The volumetric flux out of the pool can be computed from the surface area of the pool in contact with the rock matrix and the saturated hydraulic conductivity of the matrix. If the aperture of the fracture is much less than the length of the pool, most of the water exits into the matrix from the bottom of the pool when the fracture is inclined. Because the water in the pool is at a slight positive pressure, water will flow out of the pool at a rate slightly greater than K_{sat}, but for this formulation we will assume that the rate is equal to K_{sat}. The volumetric flux out of the pool becomes

$$Q_{\text{pool,out}} = L_{\text{pool}} W K_{\text{sat}} \tag{5}$$

By equating equations (4) and (5), we can determine the value of q_v, which is not known a priori and varies depending on the input flux and the fracture inclination angle

$$q_v = \frac{L_{\text{pool}} K_{\text{sat}}}{L - L_{\text{pool}}} \tag{6}$$

[22] Using the equation derived for a falling film on an inclined flat surface, the effective film thickness corresponding to a particular film flow rate can be calculated from the following equation [*Bird et al.*, 1960]:

$$\delta = \left(\frac{3 \mu Q_{\text{film}}}{\rho g W \sin \beta} \right)^{1/3} \tag{7}$$

Equations (2) and (7) are equivalent, except (7) is written in terms of the flow rate rather than the average velocity. Film fluxes and thicknesses calculated from the experimental data are discussed in the next section.

3.3.2. Measured Pool Lengths and Calculated Fluxes

[23] The pool lengths at the terminus of a 20 degree fracture were measured as a function of the input flux, and the results are presented in Table 1. Measurements of pool lengths in a 60 degree fracture are not included in the table because the pool lengths were too small to be accurately measured (<1–2 mm). The threshold flux for pooling in the 20 degree fracture occurred between 4×10^{-5} and 5×10^{-5} cm/s. The pool lengths range from 1 cm at an input flux of 5×10^{-5} cm/s to approximately 2 cm at a flux of 10×10^{-5} cm/s. The corresponding seepage fluxes using the measured pool lengths and equation (6) are summarized in Table 1 and range between 2×10^{-5} and 5×10^{-5} cm/s. The measured pool lengths were also used to calculate

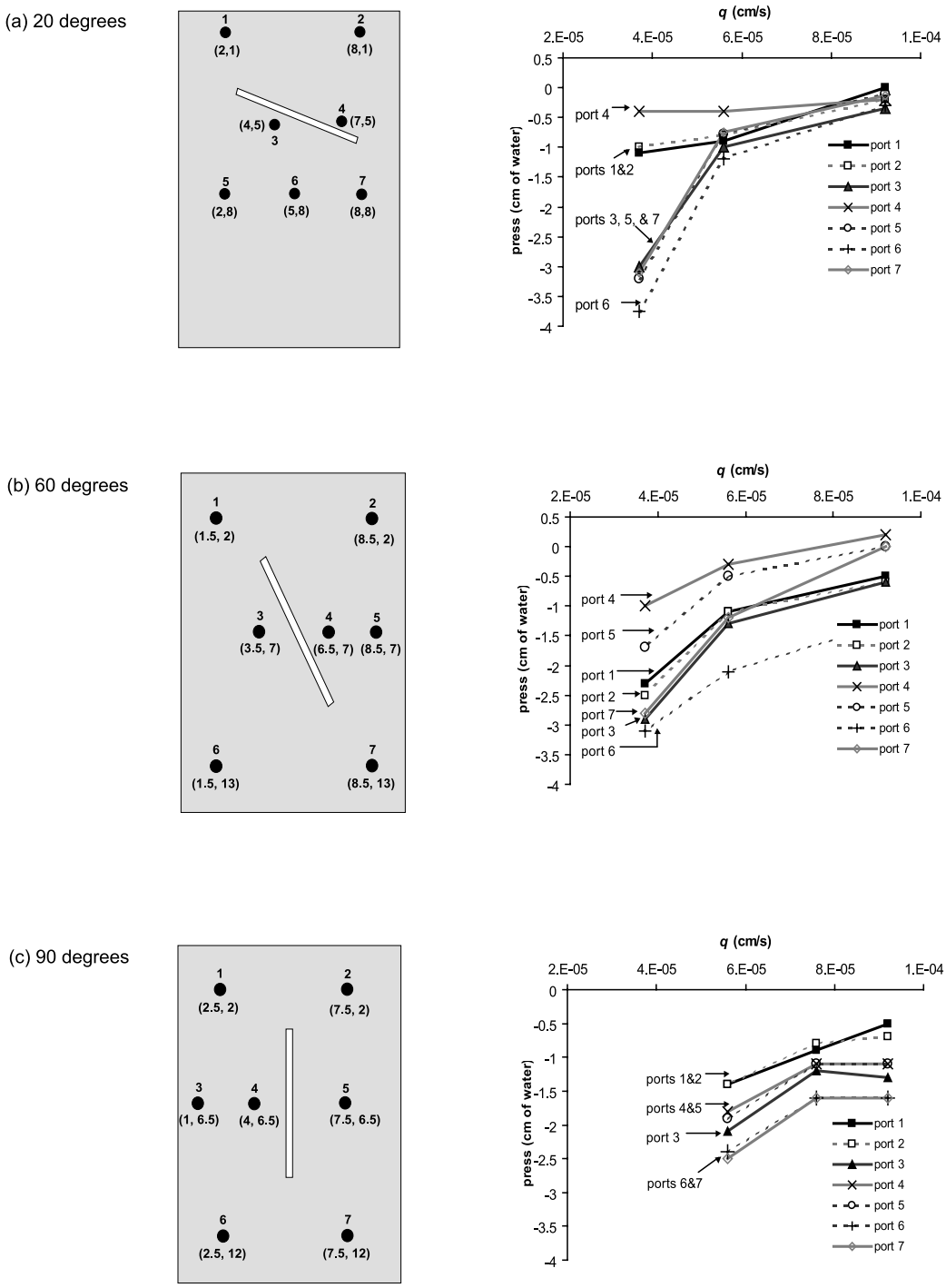

Figure 8. Pressure measurements as a function of flux (plot on right) for seven locations in the rock sample (schematic on left) with an isolated fracture oriented at (a) 20 degrees, (b) 60 degrees, and (c) 90 degrees. Values in parentheses denote tensiometer coordinates (x, z), with the origin assigned to the upper left corner of the slab.

the volumetric fluxes entering and exiting the pool (equations (4) and (5)). These values are summarized in Table 1 along with the total volumetric flux applied to the sample and the ratio of the film flow rate to the total flow rate. The calculated film flow rate was between 20 and 22% of the total flow rate. This is substantially less than the 56% of the cross-sectional area of the matrix that is intercepted by the fracture. Therefore an estimated 34–36% of the intercepted flux is diverted around the fracture, resulting in greater downward fluxes. The film thicknesses at the point where the film intersected the pool were also calculated and range from 14 to 18 μm, which is consistent with the range

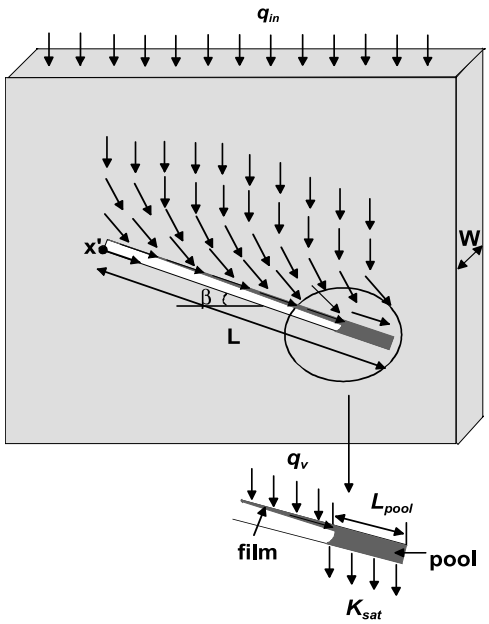

Figure 9. Flow lines near the fracture-matrix interface and film flow and pooling in an isolated fracture.

of thicknesses measured in the experiments conducted by *Tokunaga and Wan* [1997].

4. Discussion

[24] The importance of film flow and localized flow through the matrix depends on factors such as the input flux, fracture angle and aperture, matrix properties, and wettability. In this study we examined the effect of fracture angle and input flux on film flow and localized matrix flow. For a fracture at 60 degrees, we observed that preferential flow through the matrix dominated over film flow. At 90 degrees, flow through the matrix was uniform and water did not pool in the fracture, suggesting that for vertical fractures, preferential flow through the matrix and film flow may not be significant. For fractures less than 20 degrees, we anticipate that film flow and preferential flow though the matrix will both be important over a range of input fluxes, but the relative importance of these two mechanisms was not examined in this study for fractures less than 20 degrees. Localized flow through the rock matrix and film flow along isolated fractures can accelerate contaminant transport through the unsaturated zone beyond the expectations or predictions based on classical theory. These results have applications beyond that of fractured rock in the unsaturated zone. Cracks and other macropores are common in unsaturated soils and behave hydraulically like fractures [e.g., *Beven and Germann*, 1982; *Bouma*, 1991].

[25] The experiments presented in this paper were conducted using a sandstone rock with relatively high permeability and a homogeneous matrix. For different porous materials, similar flow mechanisms may occur with similar dependencies on fracture orientation and input flux. For low matrix permeability fractured materials, the contribution of matrix flow to contaminant transport may only be significant over large timescales. Film flow along inclined isolated fractures in low permeability rock may occur after a precipitation event because of the high in situ matrix saturation of low permeability rock. Fracture coatings and changes in surface wettability may affect whether film flow occurs, however.

[26] The effect of isolated fracture networks on flow may be very important. Flow through the matrix may be impacted by the network configuration, resulting in very tortuous, localized flow paths around the fracture network. If an inclined isolated fracture intersects another fracture, water flowing as a film along the inclined fracture surface may pool at the fracture intersection. Once the capillary barrier at the intersection is overcome, the accumulated water may be rapidly transported to significant depths if the intersecting fracture is nearly vertical.

[27] Fractures open to the surface may also play an important role in fast transport of water and contaminants. However, in regions with deep unsaturated zones, many of these fractures may not intersect the groundwater table since some dead-end or become filled. Therefore isolated fractures are likely to play a significant role in fast transport of contaminants when considering flow deeper in the unsaturated zone.

5. Summary and Conclusions

[28] A series of flow visualization experiments were conducted for a range of input fluxes on Berea sandstone rock samples each containing a single isolated fracture oriented at an angle between 20 and 90 degrees from the horizontal. The experiments demonstrated that two important flow mechanisms occur: (1) localized flow through the rock matrix and (2) pooling of water at the bottom of the fracture, indicating the occurrence of film flow along the isolated fracture wall. These mechanisms were observed in samples with a 20 and 60 degree fracture, but not in one

Table 1. Calculated Film Fluxes and Film Thicknesses for a Sample With a 20 Degree Fracture

q_{in}, cm/s	L_{pool}, cm	q_v, cm/s (Equation (6))	$Q_{film,in} = Q_{pool,out}$, cm^3/s (Equations (4) and (5))	$Q_{total,in}$ ($q_{in} \times A$[a]), cm^3/s	$Q_{film,in}/Q_{total,in}$	δ, μm (Equation (7))
10×10^{-5}	2.0	5.0×10^{-5}	1.3×10^{-4}	6.0×10^{-4}	0.22	18
8×10^{-5}	1.5	3.3×10^{-5}	9.5×10^{-5}	4.8×10^{-4}	0.20	16
6×10^{-5}	1.2	2.5×10^{-5}	7.6×10^{-5}	3.6×10^{-4}	0.21	15
5×10^{-5}	1.0	2.0×10^{-5}	6.4×10^{-5}	3.0×10^{-4}	0.21	14
4×10^{-5}	0.0	...	...	2.4×10^{-4}	...	...

[a] A = 0.6 cm × 10 cm.

with a 90 degree fracture. When the fracture was inclined, higher matrix pressures were measured above the isolated fracture compared to below it and higher pressures generally occurred in the regions where faster flow was observed in the visualization experiments. Pooling of water along the bottom of the fracture was observed over a wider range of input fluxes for the 20 degree fracture compared to the 60 degree one. Pool lengths measured as a function of input flux in a 20 degree isolated fracture were used to estimate the film flow rates along the isolated fracture. These rates were between 20 and 22% of the total input flow rate, indicating that a significant portion of the flow can occur as a film along the isolated fracture wall. Our experiments demonstrate that isolated fractures play an important role in accelerating flow and contaminant transport and should be accounted for when developing conceptual models of unsaturated zone flow.

[29] **Acknowledgments.** This work was funded by the National Research Council Associateship Program. Thanks are due David Stonestrom and Steven Anderson of the USGS for careful reviews of this paper.

References

Beven, K., and P. Germann, Macropores and water flow in soils, *Water Resour. Res.*, *18*(5), 1311–1325, 1982.

Bird, R. B., W. E. Stewart, and E. N. Lightfoot, *Transport Phenomena*, pp. 37–41, John Wiley, Hoboken, N. J., 1960.

Birkholzer, J., G. Li, C.-F. Tsang, and Y. Tsang, Modeling studies and analysis of seepage into drifts at Yucca Mountain, *J. Contam. Hydrol.*, *38*, 349–384, 1999.

Bouma, J., Influence of soil macroporosity on environmental quality, *Adv. Agron.*, *46*, 1–37, 1991.

Dahan, O., R. Nativ, E. M. Adar, B. Berkowitz, and Z. Ronen, Field observation of flow in a fracture intersecting unsaturated chalk, *Water Resour. Res.*, *35*(11), 3315–3326, 1999.

Dragila, M. I., A new theory for transport in unsaturated fractures: Free surface film flows, Ph.D. thesis, Univ. of Nev., Reno, May 1999.

Fabryka-Martin, J. T., A. V. Wolfsberg, A. V. Dixon, P. R. Dixon, S. Levy, J. Musgrave, and H. J. Turin, Summary report of chlorine-36 studies: Sampling, analysis and simulation of chlorine-36 in the Exploratory Studies Facility, *Rep. LA-CST-TIP-96-002*, Los Alamos Natl. Lab., Los Alamos, N. M., 1996.

Faybishenko, B., C. Doughty, M. Steiger, J. C. S. Long, T. R. Wood, J. S. Jacobsen, J. Lore, and P. T. Zawislanski, Conceptual model of the geometry and physics of water flow in a fractured basalt vadose zone, *Water Resour. Res.*, *36*(12), 3499–3520, 2000.

Glass, R. J., and M. J. Nicholl, Physics of gravity fingering of immiscible fluids within porous media: An overview of current understanding and selected complicating factors, *Geotherma*, *70*, 133–163, 1996.

Nativ, R., E. Adar, O. Dahan, and M. Geyh, Water recharge and solute transport through the vadose zone of fractured chalk under desert conditions, *Water Resour. Res.*, *31*(2), 253–261, 1995.

Nicholl, M. J., R. J. Glass, and S. W. Wheatcraft, Gravity-driven infiltration instability in initially dry nonhorizontal fractures, *Water Resour. Res.*, *30*(9), 2533–2546, 1994.

Nitao, J. J., and T. A. Buscheck, Infiltration of a liquid front in an unsaturated, fractured porous medium, *Water Resour. Res.*, *27*(8), 2099–2112, 1991.

Or, D., and M. Tuller, Flow in unsaturated fractured porous media: Hydraulic conductivity of rough surfaces, *Water Resour. Res.*, *36*(5), 1165–1177, 2000.

Philip, J. R., Asymptotic solutions of the seepage exclusion problem for elliptic-cylindrical, spheroidal, and strip- and disc-shaped cavities, *Water Resour. Res.*, *25*(7), 1531–1540, 1989.

Soll, W., and K. Birdsell, The influence of coatings and fills on flow in fractured, unsaturated tuff porous media systems, *Water Resour. Res.*, *34*(2), 193–202, 1998.

Su, G. W., J. T. Geller, K. Pruess, and F. Wen, Experimental studies of water seepage and intermittent flow in unsaturated, rough-walled fractures, *Water Resour. Res.*, *35*(4), 1019–1037, 1999.

Tidwell, V. C., R. J. Glass, and W. Peplinski, Laboratory investigation of matrix imbibition from a flowing fracture, *Geophys. Res. Lett.*, *22*, 1405–1408, 1995.

Tokunaga, T. K., and J. Wan, Water film flow along fracture surfaces of porous rock, *Water Resour. Res.*, *33*(6), 1287–1295, 1997.

Tokunaga, T. K., and J. Wan, Surface-zone flow along unsaturated rock fractures, *Water Resour. Res.*, *37*(2), 287–296, 2001.

Wang, J. S. Y., and T. N. Narasimhan, Hydrologic mechanisms governing fluid flow in a partially saturated, fractured, porous medium, *Water Resour. Res.*, *21*(12), 1861–1874, 1985.

M. I. Dragila, Department of Crop and Soil Science, Oregon State University, Corvallis, OR 97331, USA.

J. R. Nimmo, U.S. Geological Survey, Menlo Park, CA 94025, USA.

G. W. Su, Lawrence Berkeley National Laboratory, 1 Cyclotron Road, M.S. 90R01116, Berkeley, CA 94720, USA. (gwsu@lbl.gov)

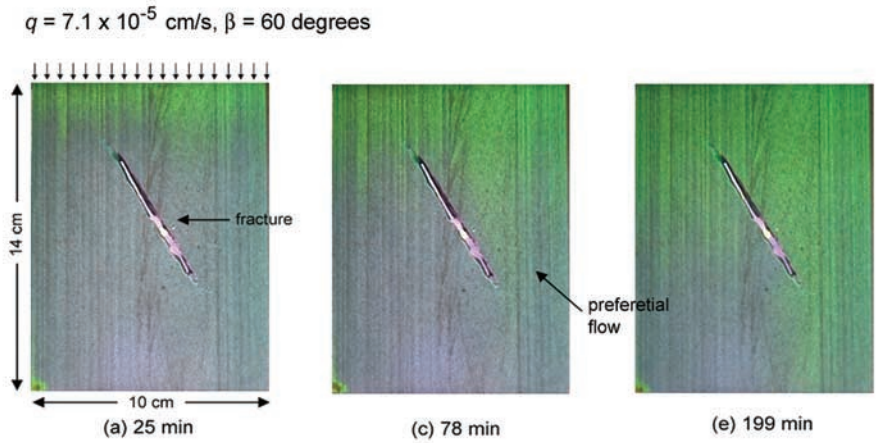

Figure 4. Water movement (green) through a slab of Berea sandstone containing a 60 degree isolated fracture. Time indicates minutes after dyed water was introduced into the sample. The q is the imposed flux density and β is the fracture angle from the horizontal.

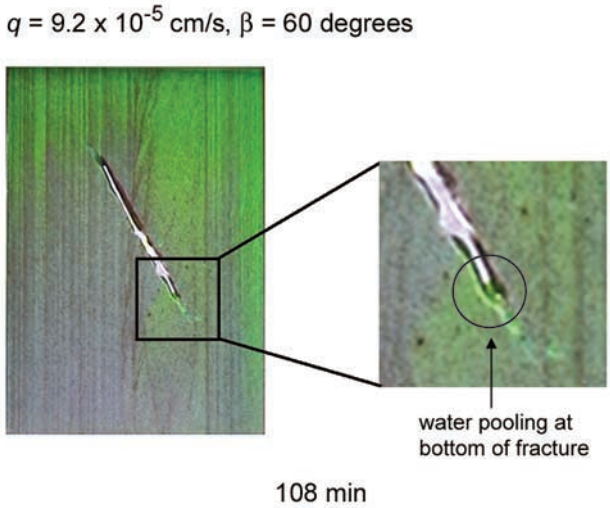

Figure 5. Water pooling at the terminus of the fracture, indication of development of free-surface film flow along the fracture walls.

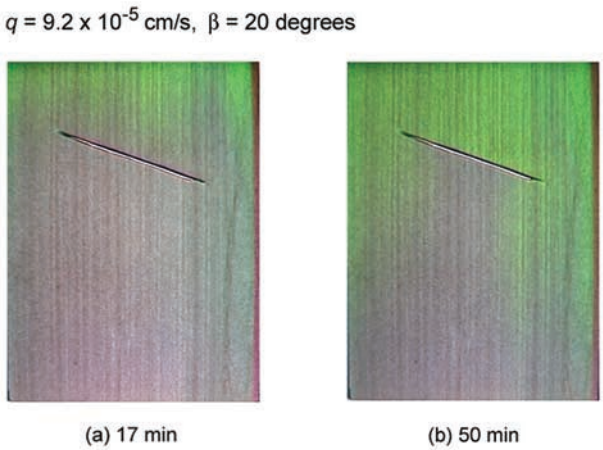

Figure 6. Flow occurs preferentially along the left and right sides of a sample containing a 20 degree isolated fracture.

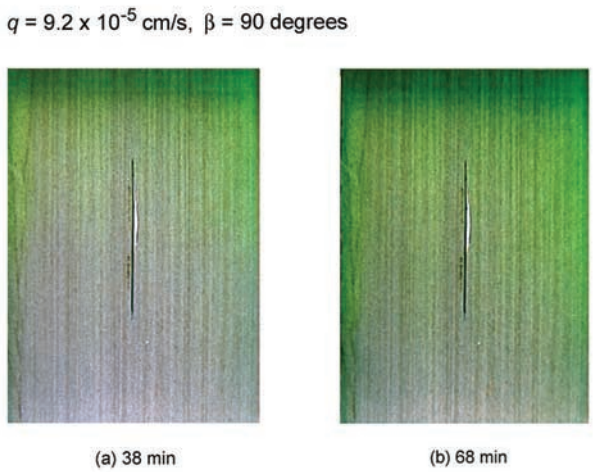

Figure 7. Flow occurs nearly uniformly along a sample containing a 90 degree isolated fracture.